Dispersion-enabled quantum state control in integrated photonics

Ryan P. Marchildon[1,*] and Amr S. Helmy[1,2]

[1]*The Edward S. Rogers Department of Electrical and Computer Engineering, University of Toronto, 10 King's College Road, Toronto, Ontario M5S 3G4, Canada*
[2]*Institute for Optical Sciences, University of Toronto, 60 St. George Street, Toronto, Ontario M5S 3G4, Canada*
Corresponding author: ryan.marchildon@mail.utoronto.ca

Integrated optics has brought unprecedented levels of stability and performance to quantum photonic circuits. However, integrated devices are not merely micron-scale equivalents of their bulk-optics counterparts. By exploiting the inherently dispersive characteristics of the integrated setting, such devices can play a remarkably more versatile role in quantum circuit architectures. We show this by examining the implications of linear dispersion in an ordinary directional coupler. Dispersion unlocks several novel capabilities for this device, including *in situ* control over photon spectral and polarization entanglement, tunable photon time ordering, and entanglement-sensitive two-photon coincidence generation. Also revealed is an ability to maintain perfect two-photon anti-coalescence while tuning the interference visibility, which has no equivalent in bulk optics. The outcome of this work adds to a suite of state engineering and characterization tools that benefit from the advantages of integration. It also paves the way for reevaluating the possibilities offered by dispersion in other on-chip devices.   © 2016 Optical Society of America

OCIS codes: (270.5585) Quantum information and processing; (130.0130) Integrated optics; (230.3990) Micro-optical devices.

http://dx.doi.org/10.1364/OPTICA.3.000243

1. INTRODUCTION

The quantum properties of light can unlock a variety of enhanced and novel technological capabilities. Among these are secure communications [1], nonclassical simulation [2], nonlocal imaging [3], and pathway-selective exciton spectroscopy [4]. Such quantum photonic technologies have traditionally been implemented on the bench top with discrete optical components. More recently, the need for improved scalability has fuelled widespread interest in the development of on-chip quantum circuits. Much of this work has concentrated on the generation [5–8], manipulation [9–12], and detection [13,14] of entangled [15] photon pairs, often with the goal of replicating tasks previously performed using bulk optics. However, integrated optical components can exhibit highly wavelength-dependent (i.e., dispersive) behavior compared to their bulk optics counterparts, and investigating whether this leads to functionalities not previously available is also an important objective. Such dispersion has been shown to provide unprecedented tailorability over the properties of two-photon states generated by engineered nonlinear interactions [16–18] in integrated waveguides. Here, we consider new ways of leveraging dispersion for the manipulation of two-photon states and their correlation properties.

Directional couplers are a common building block of integrated quantum circuits whose dispersion properties have yet to be fully exploited. They are typically implemented through the evanescent coupling of two identical waveguides and are characterized by a power splitting ratio $\eta(\lambda)$. Their primary role has been to serve as on-chip beam splitters, often to mediate quantum interference [9,10]. Due to the presence of dispersion in $\eta(\lambda)$, these same couplers can also act as a wavelength demultiplexer (WD) for specific sets of nondegenerate wavelengths, without relying on waveguide modal mismatch. In fact, dispersion can cause the coupler's behavior to transition between "ideal" beam splitter operation and "ideal" WD operation in response to either the properties of the quantum state or systematic shifts to the coupling strength. The implications this has for two-photon state manipulation has yet to be studied. We show that this attribute of directional couplers grants them a versatile set of new functionalities, which includes the post-selective tuning of spectral entanglement, entanglement-sensitive coincidence detection, and the ability to maintain perfect anti-coalescence while allowing full tunability over the two-photon interference visibility.

In what follows, we use symmetric 2 × 2 directional couplers as an example of quantum state engineering in integrated photonic systems without the loss of generality. As such, an essential step is to parameterize the coupler's response for the two-photon state in terms of generic dimensionless variables that can be mapped to any combination of coupler and state properties. The details of this parametrization are described in Supplement 1, but we introduce the key definitions here. Suppose two single-mode waveguides are coupled over a length L, such as in Fig. 1(a). For symmetric rectangular waveguides, this leads to a power splitting
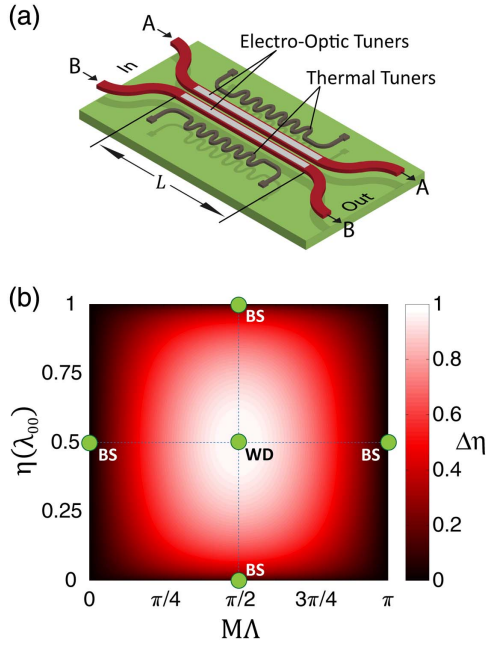
(a)

(b)

Fig. 1.   Navigating the coupler response. (a) Depiction of a generic two-port directional coupler, shown with simple implementations of thermal and electro-optic tuning for *in situ* control over $\eta(\lambda_{00})$; (b) map of possible coupler responses to a two-photon input state, as characterized by $\Delta\eta$. The coordinates labelled BS denote 50:50 beam-splitter behavior, while WD denotes perfect demultiplexing of central wavelengths λ_{01} and λ_{02}.

ratio of $\eta(\lambda) = \cos^2(\kappa(\lambda)L)$, where $\kappa(\lambda)$ is the coupling strength [19,20]. The wavelength dependence of the coupler is usually sufficiently described by its first-order coupler dispersion $M = d\kappa(\lambda)L/d\lambda$ at a reference wavelength λ_{00}, together with the value of $\eta(\lambda_{00})$. Let λ_{01} and λ_{02} be the central wavelengths of a photon pair that evolves through this coupler, with $\Lambda = |\lambda_{02} - \lambda_{01}|$ giving the nondegeneracy. Defining $\Delta\eta = |\eta(\lambda_{02}) - \eta(\lambda_{01})|$ allows the coupler response to be classified as beam splitter-like for $\Delta\eta \to 0$ or WD-like for $\Delta\eta \to 1$. An illustrative example of a practical dispersive coupler design is provided in Supplement 1.

The space of all possible $\Delta\eta$ is spanned by $\eta(\lambda_{00})$ and the dimensionless product $M\Lambda$. This has been plotted in Fig. 1(b), assuming $\lambda_{00} = (\lambda_{01} + \lambda_{02})/2$ and negligible higher-order coupler dispersion (see Supplement 1). This plot provides a useful guide for relating the results of this paper to transitions between beam splitter and WD behavior. A special condition, $\eta(\lambda_{01}) + \eta(\lambda_{02}) = 1$, occurs along the lines $\eta(\lambda_{00}) = 0$ and $M\Lambda = \pi/2$, and corresponds to the splitting ratios $\eta(\lambda_{01})$ and $\eta(\lambda_{02})$ being antisymmetric about the 50:50 splitting value $\eta = 0.5$. This will turn out to have important implications for tasks involving photon anti-coalescence.

2. DISPERSION-ENABLED CAPABILITIES

A. Tunable Spectral Entanglement

Suppose two nondegenerate photons enter a directional coupler from a single input port so that the input state takes the form $|\psi\rangle_{\text{in}} = |\lambda_{01}\rangle_j|\lambda_{02}\rangle_j$, where $j \in \{A, B\}$. The two-photon state at the output of the coupler is then post-selected for outcomes where the photons exit from different waveguides (i.e., separated).
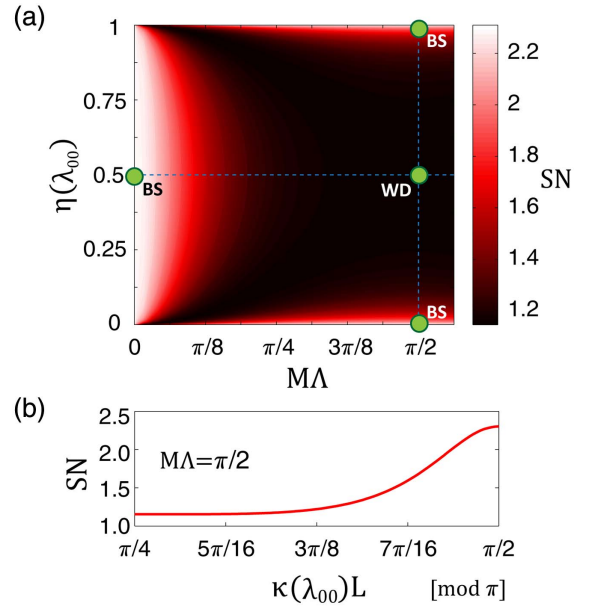
(a)

(b)

Fig. 2.   Tunability of output state entanglement. (a) Dependence of Schmidt number on the coupler response for post-selected outcomes where the photons are found in different waveguides. The maximum value of SN = 2.31 corresponds to the input state entanglement. (b) Slice along $M\Lambda = \pi/2$, plotted in terms of $\kappa(\lambda_{00})$.

Depending on the coupler response, the output waveguide taken by a given photon can reveal information about that photon's spectral properties, which in turn alters the spectral entanglement of the post-selected output state. A WD-like response with $\Delta\eta = 1$ predetermines which photon emerges from each output port. This leads to an output state of the form $|\psi\rangle_{\text{out}} = |\lambda_{01}\rangle_A|\lambda_{02}\rangle_B$ (or $|\psi\rangle_{\text{out}} = |\lambda_{01}\rangle_B|\lambda_{02}\rangle_A$, depending on the input port), where entanglement of the central wavelengths is lost. On the other hand, a beam splitter-like response with $\Delta\eta = 0$ leads to the superposition $|\psi\rangle_{\text{out}} = [|\lambda_{01}\rangle_A|\lambda_{02}\rangle_B + |\lambda_{01}\rangle_B|\lambda_{02}\rangle_A]/\sqrt{2}$, where the full spectral entanglement of the input state is retained. By controlling $\Delta\eta$ through the selection of M or $\eta(\lambda_{00})$ (and thus controlling, effectively, the amount of spectral information known about the output state), a directional coupler can select any level of entanglement between these extremes.

Figure 2 shows how the choice of M and $\eta(\lambda_{00})$ can tailor spectral entanglement in the post-selected output state (see Appendix A and Supplement 1 for calculation details). Spectral entanglement has been quantified using the Schmidt number (SN) [21,22], which has a minimum value of unity in the absence of entanglement, and increases with greater entanglement. The input state used in this example has $\Lambda = 10$ nm, SN = 2.31, and equal FWHM intensity bandwidths of $\Delta\lambda = 1$ nm for the photon marginal spectra. It is modeled after a Type-I spontaneous parametric downconversion (SPDC) process [23] with a degeneracy wavelength of $\lambda_{00} = 1550$ nm and pump bandwidth of $\Delta\lambda_P = 0.25$ nm. As the coupler response moves away from the beam splitter-like coordinates and toward the WD-like coordinate at $(M\Lambda = \pi/2, \eta(\lambda_{00}) = 0)$, the Schmidt number of the output state smoothly transitions from its input value of SN = 2.31 down to a value of SN $\simeq$ 1.15. Note that some spectral entanglement remains at the WD-like coordinate even though the output paths reveal the central wavelengths.

This is because the photon spectra are still inherently anticorrelated about their central wavelengths, due to energy and momentum conservation in the pair generation process. Such residual entanglement vanishes as $\Delta\lambda \to 0$.

In situ tuning of the Schmidt number becomes possible through active control of $\eta(\lambda_{00})$. Effectively, this prepares states of the form $|\psi\rangle_{out} = [|\lambda_{01}\rangle_A|\lambda_{02}\rangle_B + \mu|\lambda_{01}\rangle_B|\lambda_{02}\rangle_A]/\sqrt{1 + \mu^2}$ with a tunable value of μ. We emphasize that this tuning occurs post-generation, without requiring changes to pump bandwidth, nonlinear interaction length, or any other parameters affecting the photon pair generation process. This makes it particularly well suited for tailoring spectral entanglement in a monolithically integrated setting, in applications where the photons remain path-distinguishable. Control of $\eta(\lambda_{00})$, and thereby the Schmidt number, can be achieved electro-optically or thermally by modifying the waveguide core-cladding index contrast to systematically shift $\kappa(\lambda_{00})$. Other potential tuning methods include the quantum-confined Stark effect [24,25] and, for certain fiber-based coupler assemblies, a micrometer-controlled waveguide separation [26]. Operation along the line $M\Lambda = \pi/2$ offers the most precise control over entanglement at any nonzero Λ. The value of M is fixed but can be tailored through a judicious design of the coupler dimensions and material system. Note that, since M scales with L, dispersion can be enhanced by increasing the 50:50 coupling length beyond its minimum necessary value of $L = \pi/(4\kappa(\lambda_{00}))$.

This tuning approach also provides control over polarization entanglement, since correlations in the spectral and polarization degrees of freedom are coupled [22], except in the special case of maximal polarization entanglement. A state's polarization entanglement can be quantified using its concurrence C [27,28], with $C = 0$ and $C = 1$ indicating minimal and maximal entanglement, respectively. As the state Schmidt number increases, polarization entanglement tends to decrease, and vice versa [22]. This inverse relationship between SN and C allows for the on-chip preparation of non-maximally entangled states $|\psi\rangle = (|H, V\rangle + r \exp i\phi|V, H\rangle)/\sqrt{1 + r^2}$ with a tunable value of $r < 1$, with r related to the concurrence by $C = 2r/(1 + r^2)$. Such states offer significant advantages over maximally entangled states in certain applications such as closing the detection loophole in quantum nonlocality tests [29].

The tunable spectral entanglement we present may also have useful capabilities for two-photon spectroscopy [30] and light-induced matter correlations [31,32]. In these applications, the time ordering of when each photon reaches the sample can affect the two-photon absorption probability. This is because a particular two-photon transition can have pairings of absorption pathways corresponding to whether λ_{01} or λ_{02} is absorbed first. For some systems, when both time orderings are permitted by the incident light, these pathways destructively interfere to suppress the two-photon absorption probability, as is the case for two uncoupled two-level atoms [31]. Such transitions can thus be selectively controlled by changing which time orderings (and hence absorption pathways) are allowed.

As illustrated in Fig. 3, control over the allowed time orderings is achievable by placing a time delay in one path (e.g., path A) and tuning μ by tuning the coupler parameter $\eta(\lambda_{00})$. Suppose $\mu = 0$ [Fig. 3(b)] so that the post-selected state at the coupler output is $|\psi\rangle_{out} = |\lambda_{01}\rangle_A|\lambda_{02}\rangle_B$. In this case, λ_{01} is always delayed relative to λ_{02}. Hence, only one set of time-ordered pathways is allowed.
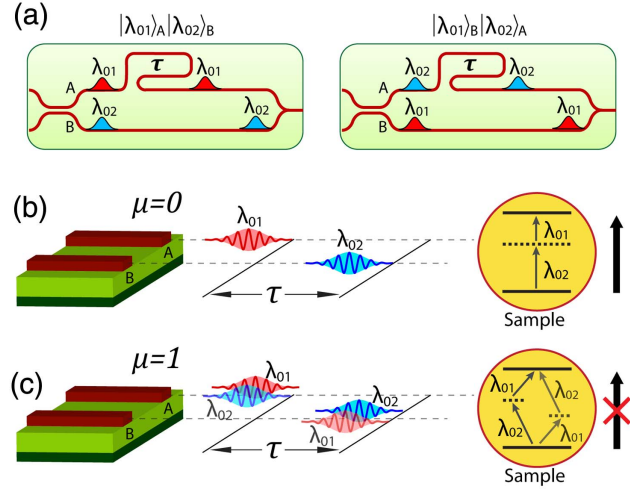

Fig. 3. Probing matter with tunable time ordering. (a) Photons leaving the coupler from different output ports have two possible pathways: $|\lambda_{01}\rangle_A|\lambda_{02}\rangle_B$ or $|\lambda_{01}\rangle_B|\lambda_{02}\rangle_A$. These coincide temporally and hence are mutually coherent. The photon in waveguide A is then temporally delayed by an interval τ relative to its twin photon in waveguide B, so that one photon always arrives at the sample before the other. The wavelength of the delayed photon depends on whether the pathway was $|\lambda_{01}\rangle_A|\lambda_{02}\rangle_B$ or $|\lambda_{01}\rangle_B|\lambda_{02}\rangle_A$. (b) For $\mu = 0$, only the $|\lambda_{01}\rangle_A|\lambda_{02}\rangle_B$ pathway is allowed, such that the photon of wavelength λ_{02} is always absorbed first. (c) For $\mu = 1$, the superposition permits two absorption pathways: λ_{02} followed by λ_{01}, and λ_{01} followed by λ_{02}. In certain systems [31] where it is not possible to distinguish which of these pathways led to the final state of the sample, the pathways destructively interfere to suppress the two-photon absorption probability. Note that at $\mu = 1$ the pathways $|\lambda_{01}\rangle_A|\lambda_{02}\rangle_A$ and $|\lambda_{01}\rangle_B|\lambda_{02}\rangle_B$ are also present due to nondeterministic separation (the coupler behaves as a beam splitter rather than a WD), yielding photons with no relative delay. These are not time ordered but do support both absorption pathways and therefore compliment the path-interference effects.

On the other hand, when $\mu = 1$ [Fig. 3(c)] so that $|\psi\rangle_{out} = [|\lambda_{01}\rangle_A|\lambda_{02}\rangle_B + |\lambda_{01}\rangle_B|\lambda_{02}\rangle_A]/\sqrt{2}$, the delay is applied in superposition to either λ_{01} or λ_{02}, and hence both sets of time-ordered pathways are allowed.

Such control over the time ordering adds to the versatility of a single on-chip light source for manipulating and probing two-photon processes, such as controlling the degree to which biexciton transitions may be blocked [4]. Note that the ability to selectively excite a single absorption path (e.g., using $\mu = 0$) is only possible with quantum light sources. Classical sources have no intrinsic time ordering and hence will excite both paths equally (as with $\mu = 1$). A tunable dispersive coupler thus allows the sample's behavior for both the classical and nonclassical conditions to be directly compared, without the need to change the light source and with virtually no disruption to the experimental setup.

B. Perfect Anti-Coalescence with Tunable Visibility

Control over two-photon path correlations is another important ability for quantum photonics. In this section, we start by exploring how such correlations can be impacted by dispersion. We then describe how this enables conditions with no bulk optics equivalent; namely, perfect photon anti-coalescence that remains independent of the visibility of interference effects, even as this visibility is tuned via $\eta(\lambda_{00})$ or $M\Lambda$. Later in Section 2.C, we will

highlight possible applications for the dispersion-unlocked correlation behavior that underscore the breadth of capabilities that a single dispersive coupler can provide.

Path correlations are commonly engineered using quantum interference [10,12,33–36]. In the famous Hong—Ou—Mandel effect [33], two photons enter a 50:50 beam splitter from different input paths (antibunched), and coalesce to exit as a bunched state where they are most likely to be found in the same output path. Ideally the antibunched (i.e., separated) outcome probability becomes $P_S = 0$ under conditions of maximal interference, compared to the "classical" value of $P_S^C = 0.5$ if interference were completely absent. The reverse process, called anti-coalescence, wherein $P_S \to 1$, is useful for providing interference-facilitated pair separation (IFPS) to separate photons generated by integrated sources [12,36,37]. Note that the subscript S is used to delineate these from probabilities corresponding to bunched (i.e., non-separated) outcomes; this is detailed further in Supplement 1. The two-photon interference can be quantified by the interference visibility $V_S = |P_S^I|/P_S^C$, where $P_S^I = P_S - P_S^C$ represents the contribution of quantum interference toward the antibunched outcome probability.

We shall now look specifically at anti-coalescence. While perfect coalescence requires V_S to be unity (see Supplement 1), coupler dispersion can lift this restriction for anti-coalescence. As we shall see, for the first time V_S can be made to have any arbitrary value between 0 and 1 while the separation probability is kept constant at $P_S = 1$. Anti-coalescence requires a path-entangled input state of the form

$$|\Psi\rangle = [|\psi\rangle_A|0\rangle_B + e^{-i\theta}|0\rangle_A|\psi\rangle_B]/\sqrt{2}, \qquad (1)$$

where $|0\rangle$ refers to vacuum, $|\psi\rangle_j$ represents a photon pair in path j, and θ is a relative phase shift. Such states can be generated by coherently pumping two sources of photon pairs, as seen in Refs. [12] and [36]. This places no restrictions on the tunability of the photon pair sources. The spectral properties of $|\psi\rangle_j$ are described by the biphoton amplitude (BPA) $\phi^j(\omega_1, \omega_2)$. We will assume perfect path indistinguishability such that $\phi^A(\omega_1, \omega_2) = \phi^B(\omega_1, \omega_2) \equiv \phi(\omega_1, \omega_2)$.

Figure 4 shows how P_S, P_S^C, P_S^I, and V_S change as a function of the coupler parameters when the relative phase shift is either $\theta = 0$ or $\theta = \pi$. These plots have been generated for a co-polarized input state from Type-I SPDC having $\Delta\lambda = 0.25$ nm, $\Delta\lambda_P = 0.1$ nm and a degeneracy wavelength of $\lambda_{00} = 780$ nm (see Appendix A). The dependence of these on photon bandwidth will be discussed in Section 2.C. The value of $|P_S^I|$ is maximal at coordinates where the coupler responds as a 50:50 beam splitter, and minimal when it responds as a WD. The "classical" probability P_S^C follows roughly the opposite trend, obtaining its maximal value of $P_S^C = 1$ for a WD-like response, and decreasing to $P_S^C = 0.5$ for beam splitter-like responses. Curiously, along the lines $\eta(\lambda_{00}) = 0.5$ and $M\Lambda = \pi/2$, changes to P_S^C and $|P_S^I|$ are in perfect balance such that their sum always equals unity. This balancing is associated with the condition $\eta(\lambda_{01}) + \eta(\lambda_{02}) = 1$, which leads to $P_S = 1$ and hence perfect anti-coalescence (i.e., deterministic separation) along either $\eta(\lambda_{00}) = 0.5$ or $M\Lambda = \pi/2$, selected through the choice of θ. Along these two lines, the interference visibility V_S varies smoothly between 0 and 1. By operating at $M\Lambda = \pi/2$ with $\theta = \pi$, and actively controlling $\eta(\lambda_{00})$ through thermal or electro-optic tuners, any value of V_S can be selected while maintaining a perfect separation

fidelity. Note that, unlike before, this does not alter the spectral entanglement of post-selected output states, due to the presence of path entanglement at the input.

We have just described how coupler dispersion enables the possibility of tuning V_S while maintaining $P_S = 1$. The applications of this capability are not yet known, but its novelty warrants further exploration. It also serves as an example of how integrated components, through their inherent dispersive properties, can access behaviors that bulk bench-top components cannot. Further to this, we now highlight other features of the dispersion-unlocked behavior that have potential applications for state characterization.

C. Opportunities for State Characterization

1. Entanglement-Sensitive Coincidence Detection

For most permutations of coupler and state attributes, P_S is accurately described by the behavior in Fig. 4. However, deviations from the values of P_S shown can occur when the dimensionless product $M\Delta\lambda$, involving coupler dispersion and photon bandwidth, becomes large. These are described in full in Supplement 1. Fig. 5 indicates that the extent of these deviations depends not only on $M\Delta\lambda$, but also on the spectral entanglement of the input state. This opens up the possibility of discerning the Schmidt mumber of the input state from the antibunched coincidence count rate at the coupler output, which is proportional to P_S.

The results in Fig. 5 were calculated for degenerate input states having $\Lambda = 0$ nm, $\Delta\lambda = 10$ nm, $\lambda_{00} = 780$ nm, and $\theta = 0$. The product $M\Delta\lambda$ was swept by varying M, with $\eta(\lambda_{00}) = 0.5$ kept constant. Input state entanglement was controlled through the Type-I SPDC pump bandwidth $\Delta\lambda_P$ (see Appendix A and Supplement 1). In the limit of $M\Delta\lambda \to 0$, the above calculation parameters give $P_S = 1$, in agreement with Fig. 4(e). Larger values of $M\Delta\lambda$ lead to decreases in P_S. However, increasing the SN of the input state has the effect of asymptotically restoring P_S to unity.

This behavior can be understood by examining Eqs. (A.3)–(A.9) in Appendix A. The probability P_S is determined from a sum over all possible combinations of frequencies $\omega_1 = 2\pi c/\lambda_1$ and $\omega_2 = 2\pi c/\lambda_2$ weighted by the BPA. When the state is spectrally uncorrelated (i.e., SN = 1), the combinations of $\eta(\lambda_1)$ and $\eta(\lambda_2)$ contributing to this sum are not necessarily equidistant from $\eta(\lambda_{00}) = 0.5$ and hence can deviate from the $\eta(\lambda_1) + \eta(\lambda_2) = 1$ condition required for perfect anti-coalescence. However, when the photons are spectrally anticorrelated due to entanglement, the BPA restricts all contributing λ_1, λ_2 combinations to be approximately equidistant from λ_{00}, which acts to restore the splitting ratio antisymmetry. Larger products of $M\Delta\lambda$ allow P_S to be more severely degraded because a greater proportion of the nonvanishing λ_1, λ_2 combinations are able to violate the antisymmetry. Only in the limit of $\Delta\lambda \to 0$, where the state is entirely described by the central wavelengths λ_{01} and λ_{02}, is the splitting ratio antisymmetry condition strictly enforced.

The bandwidth and entanglement sensitivity of P_S grants dispersive couplers additional capabilities for state characterization. For example, dispersive couplers could empower a simple, fast, all-integrated technique for measuring the Schmidt number of an ensemble of states without needing to perform full state tomography to reconstruct the BPA. Fig. 6 describes how this can be implemented. In this case, we show the photons being
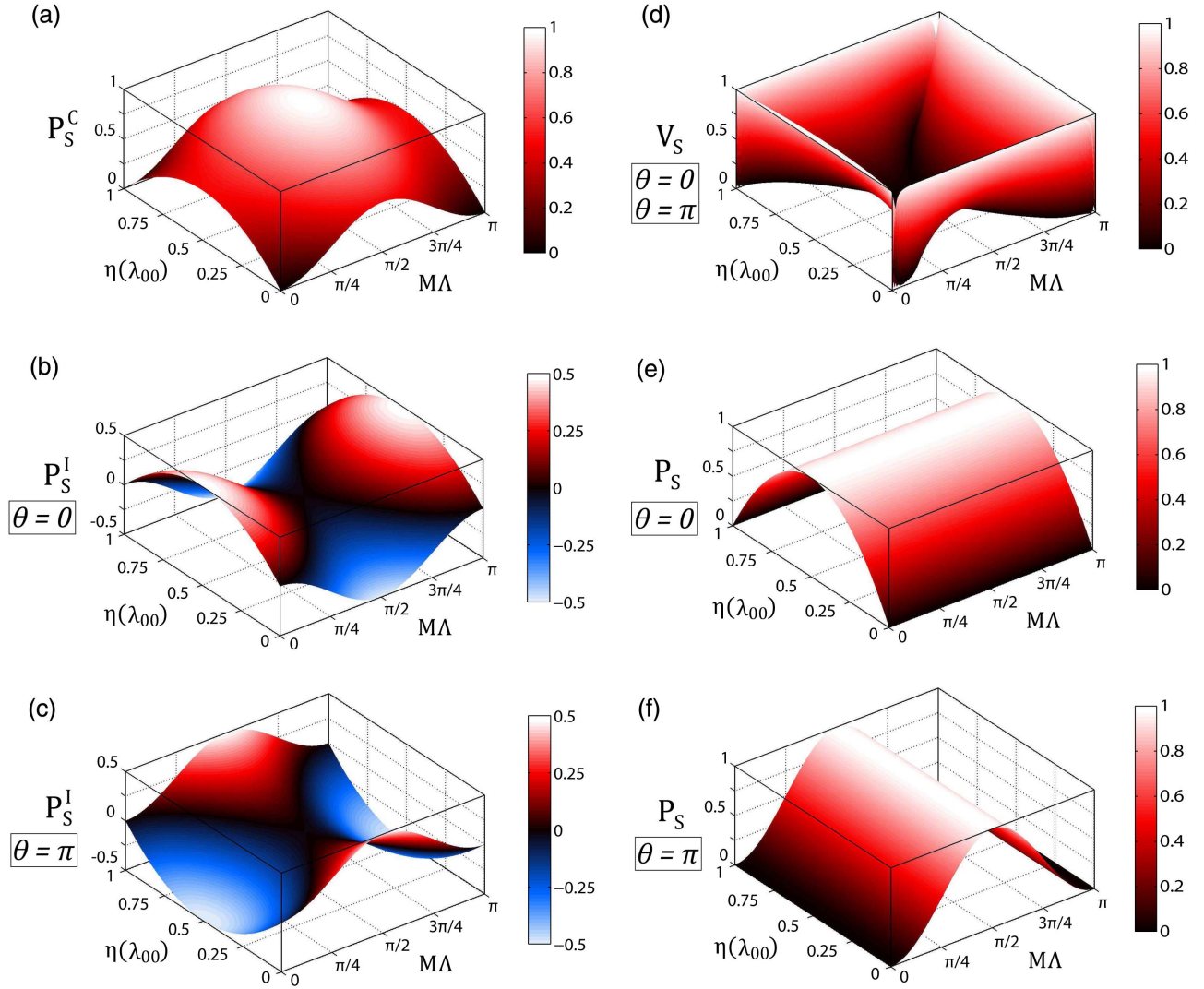
Fig. 4. Dependence of two-photon path correlations on the coupler response. Calculations depict (a) the "classical" separation probability, (b)–(c) the contribution of quantum interference, (d) the resultant interference visibility, and (e)–(f) total separation probability. Toggling the phase shift from $\theta = 0$ to $\theta = \pi$ leads to a sign change for P_S^I but leaves its magnitude $|P_S^I|$ unaltered. This sign change, in turn, toggles the line of maximal P_S between $\eta(\lambda_{00}) = 0.5$ and $M\Lambda = \pi/2$, respectively.
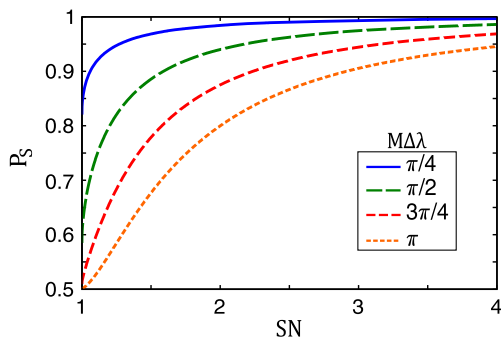

Fig. 5. Dependence of P_S on entanglement. The calculated two-photon separation probability is shown as a function of the input state Schmidt number for $M\Lambda = 0$, $\eta(\lambda_{00}) = 0.5$, $\theta = 0$, and $\Delta\lambda = 10$ nm, at several values of $M\Delta\lambda$. For SN > 4 (not shown), each curve asymptotically approaches unity.

characterized immediately after leaving the source, in the context of source calibration. However, they could also be measured after interacting with a bath or system. This could be helpful, for example, in metrological applications where the Schmidt number is monitored as an indication of state purity and hence the interaction under investigation. To obtain SN, first the marginal photon spectra are measured with a waveguide-assisted spectrograph method [38] that uses chromatic group velocity dispersion (GVD) to map spectral components to time-of-arrival at a single-photon detector. Next, provided M is known, the values of $\Delta\lambda$ and Λ measured in the first step are used to discern SN from standard two-photon coincidence measurements at the coupler outputs. The sensitivity of the technique diminishes as the photons are made narrowband or increasingly entangled, but can be enhanced by designing the coupler to have M as large as possible.

Obtaining SN by previous methods would require a measurement of the full BPA, which hinges on the spectral resolution of
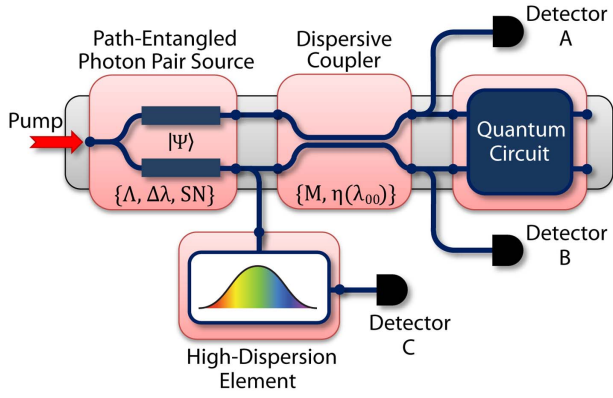
Fig. 6. All-integrated SN measurement. To apply the technique, the photon pairs must be in the generic path-entangled state $|\Psi\rangle$ of Eq. (1). The relative phase is ideally $\theta = 0$; for other values of θ, P_S is less sensitive to SN. To measure SN, the state is sampled at three locations (shown as Y-junctions for simplicity). Detectors A and B sample the two-photon statistics at the coupler output to obtain P_S. Detector C obtains spectrographs, and hence Λ and $\Delta\lambda$, by sampling $|\Psi\rangle$ via a high-dispersion element such as a fiber or a waveguide grating operated near its band edge. It is sufficient to measure these spectrographs from only one of the source output paths, since the photon pair properties are assumed to be path-indistinguishable (i.e., $|\psi\rangle_A = |\psi\rangle_B$). The data obtained for Λ and $\Delta\lambda$ (together with the dispersive coupler attributes) can then be used to map the measured P_S to a corresponding value of SN (see Fig. 5).

Fig. 7. State characterization with a multipurpose dispersive coupler. A path superposition of the form $|\Psi\rangle$ (Eq. A.1) is created through coherent pumping of two waveguide sources of photon pairs (e.g., generated via parametric downconversion [37]). A tunable Mach–Zehnder interferometer (MZI) allows the relative time delay to be set to either zero ($\phi_\tau = 0$) or τ ($\phi_\tau = \pi$). Pump power can be adjusted between paths via ϕ_p to compensate for asymmetric losses when the delay of τ is implemented. Unconverted pump photons are removed using ring filters. MZIs at the output can be toggled ($\phi_{A(B)} = \pi$) to sample the two-photon correlations with single-photon detectors. The rate of detection coincidences for zero time delay and a delay of τ can be used to determine V_S, which in turn reveals $M\Lambda$. The dispersive directional coupler must have $\eta(\lambda_{00}) = 1/2$ for this measurement. Note that adding electro-optic or thermal tuners to the dispersive coupler can enable arbitrary control over V_S by tuning $\eta(\lambda_{00})$. Spectral-entanglement tuning is also possible when ϕ_p is set to deliver pump power to only one of the two photon pair sources.

the measurement system. Measuring the BPA entirely on chip is possible using spectrographs [38], but its resolution can be severely limited by detector timing jitter. In comparison, precise values of $\Delta\lambda$ and Λ for the coupler-assisted technique are more easily obtained, in part due to the straightforward use of interpolation to increase confidence in these values, but also because uncertainties from the limited spectral resolution enter only in one axis, as opposed to two. Hence, the trade-offs between the number of measurements, the total measurement time, and precision in SN scale more favorably for the coupler-assisted technique. A direct, rapid, and precise measurement of SN would be particularly useful for the real-time monitoring of sources where SN is tunable [39] and is being used as a control parameter [32]. Additionally, it would be advantageous for monitoring a stream of states whose properties reveal real-time information about a dynamic system or environment.

The converse functionality—estimating the photon bandwidth for a known Schmidt number—could also be useful, in the context of indistinguishable pure photons having tunable attributes [40,41]. As long as the SN remains reasonably close to unity, $\Delta\lambda$ could be measured entirely on chip using only the coupler and coincidence detectors, without the need for tunable bandpass filters, GVD fibers, or spectrometer capabilities. Presently, highly bandwidth-tunable pure photons can be generated in a free-space setup [41], but recent trends toward integration suggest that this capability may eventually be available in a monolithic platform, where on-chip characterization would be helpful for source calibration and monitoring drift.

2. Versatility of Dispersive Couplers

Since couplers are already an essential on-chip device, the state characterization capabilities granted to them by dispersion can be exploited with minimal increase to the circuit complexity
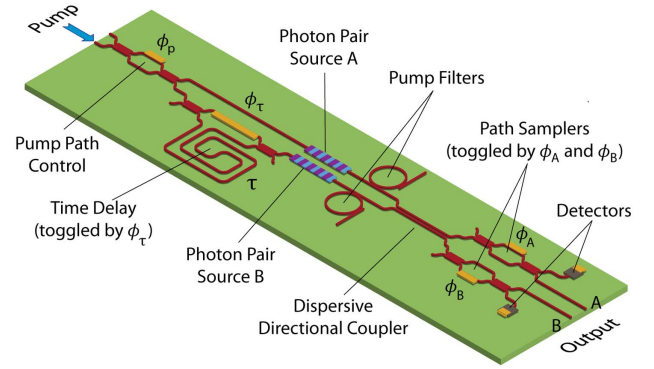
or footprint. This allows dispersive couplers to provide an extremely versatile set of functionalities in a compact form factor, which the following example highlights. Consider the reconfigurable circuit in Fig. 7. The dispersive coupler in this circuit can serve several purposes. It can provide IFPS to deterministically separate the photons at the coupler output. With the addition of electro-optic or thermal tuning, it can also be utilized for other previously described state engineering functionalities, such as tunable spectral entanglement. On top of this, the circuit could easily be modified for coupler-based SN measurements by tapping photon source B with a high-dispersion element and an additional detector, as per Fig. 6. Accomplishing all of these tasks through a single dispersive coupler may help to make most efficient use of precious on-chip real estate.

Even without adding a tap to source B for a spectrograph measurement, the circuit in Fig. 7 can already access some information about the state. The relationship between V_S and Λ described in Section 2.B provides a route for measuring the nondegeneracy Λ of an ensemble of states entirely on chip. This requires the toggling of a time delay τ between the dispersive coupler input paths. The interference visibility is obtained from $V_S = |R_0/R_\tau - 1|$, where R_0 is the coincidence count rate at zero time delay (as measured by on-chip single photon detectors), and R_τ is the coincidence rate at a time delay τ that is much larger than the two-photon coherence time (see Appendix A). Provided M is known, this value of V_S can be mapped back to the state nondegeneracy Λ, as per Fig. 4(d). This technique is best applied to narrowband photons since the sensitivity of V_S to Λ decreases as $M\Lambda$ becomes large.

3. CONCLUSIONS

Integrated couplers are already becoming a key building block of photonic quantum circuits. This is partly because they offer greater stability and scalability than bulk-optics beam splitters and other bench-top components. It is also because the highly precise micron-scale fabrication of such couplers helps eliminate path-length mismatches and other path asymmetries, which is critical for achieving high-fidelity quantum interference [42]. However, in addition to these known benefits, our work has revealed an as-of-yet untapped potential for integrated couplers to be utilized in a more versatile way, far beyond their traditional role as a beam splitter substitute.

We found that harnessing the full dispersion properties of an integrated directional coupler unlocks many novel capabilities for the device. These include tunable photon entanglement and time ordering, as well as bandwidth-sensitive and entanglement-sensitive two-photon effects that can be exploited for state characterization. Some of these capabilities can be achieved in bulk optics, but not with the convenience nor stability that this integrated approach provides. Yet others have no bulk-optics counterpart, such as the ability to fully tune the two-photon interference visibility (i.e., the sensitivity to time delays at the coupler input) while maintaining a constant flux of separated (i.e., anticoalesced) photon pairs. Particularly remarkable is that all of these functionalities can be provided by a single integrated coupler, making it a versatile yet compact tool for both state engineering and on-chip state characterization. This is made possible by the capacity of dispersive couplers to smoothly transition between the extremes of beam splitter and wavelength-demultiplexer behavior, in a manner without parallel in bulk optics.

Ultimately, we have shown that conventional integrated optics devices can have much more to offer quantum optics if reevaluated in unconventional ways. Our analysis can be extended to provide a fresh look at several other coupler types and the additional capabilities their dispersive characteristics might offer. These include multimode interferometers and rings, as well as atypical coupler geometries with more exotic transfer functions [43]. Cavity-based couplers may also have interesting uses when examined beyond the identical-photon regime [44]. This work also lays foundations for studying the implications of dispersion in coupled waveguide arrays [45] and three-dimensional tritters [46]. Such systems can be considered not only for two-photon phenomena, but also for engineering higher-order path correlation effects involving multi-pair production or multiple sources.

APPENDIX A

State Representation. A co-polarized pair with both photons beginning in waveguide j can be represented by the pure state

$$|\psi\rangle_j = \int d\omega_1 d\omega_2 \phi^j(\omega_1, \omega_2)\hat{a}^{j\dagger}(\omega_1)\hat{a}^{j\dagger}(\omega_2)|\text{vac}\rangle, \quad \textbf{(A.1)}$$

where $\hat{a}^{j\dagger}(\omega)$ is the canonical mode creation operator for waveguide j. The BPA is normalized according to $\int d\omega_1 d\omega_2 |\phi^j(\omega_1, \omega_2)| = 1$. Rather than generating the BPA from device-specific mode dispersion parameters [23,47], it is more convenient to define the BPA directly in terms of the photon bandwidths and central wavelengths of interest. A BPA that mimics the output of a Type I SPDC process can be constructed from

$$\phi(\omega_1, \omega_2) = \phi_P(\omega_1 + \omega_2)[\phi_1(\omega_1)\phi_2(\omega_2) + \phi_2(\omega_1)\phi_1(\omega_2)], \quad \textbf{(A.2)}$$

where $\phi_n(\omega)$ are the marginal photon spectra and $\phi_P(\omega_1 + \omega_2)$ is the pump spectrum. This construction satisfies the necessary exchange symmetry and has all of the key qualitative features of a typical Type I BPA computed from SPDC theory. The marginal spectra were Gaussian and defined in terms of wavelength as $\phi_n(\lambda) = \exp(-2\ln 2[\lambda - \lambda_{0n}]^2/\Delta\lambda^2)$, with equal FWHM intensity bandwidths of $\Delta\lambda$. The pump spectrum was also Gaussian with a FWHM intensity bandwidth of $\Delta\lambda_P$. Narrowing $\Delta\lambda_P$ below $\Delta\lambda$ has the effect of increasing the spectral correlations, and hence Schmidt Number, of the two-photon state.

Evolution through a directional coupler. Consider the evolution of the pure state $|\Psi\rangle$ of Eq. (A.1) through a directional coupler of length L and coupling strength $\kappa(\omega)$. It is assumed that the output remains in a pure state. Let $\hat{b}^j(\omega)$ represent the mode operators at the coupler output. These are related to the input mode operators by

$$\begin{bmatrix} \hat{b}^{A\dagger}(\omega) \\ \hat{b}^{B\dagger}(\omega) \end{bmatrix} = \begin{bmatrix} \cos(\kappa(\omega)L) & i\sin(\kappa(\omega)L) \\ i\sin(\kappa(\omega)L) & \cos(\kappa(\omega)L) \end{bmatrix} \begin{bmatrix} \hat{a}^{A\dagger}(\omega) \\ \hat{a}^{B\dagger}(\omega) \end{bmatrix}. \quad \textbf{(A.3)}$$

Note that the magnitude of the matrix elements in Eq. (A.3) are related to the power-splitting ratio by $|\cos(\kappa(\omega)L)| = [\eta(\omega)]^{-1/2}$ and $|\sin(\kappa(\omega)L)| = [1 - \eta(\omega)]^{-1/2}$. Using this transformation, the state BPAs at the output of the coupler can be written as

$$\Phi^{j\to pq}(\omega_1, \omega_2) = \phi^j(\omega_1, \omega_2)G^{j\to p}(\omega_1)G^{j\to q}(\omega_2), \quad \textbf{(A.4)}$$

where

$$G^{j\to q}(\omega) = \begin{cases} \cos(\kappa(\omega)L), & \text{if } j = q, \\ \sin(\kappa(\omega)L), & \text{if } j \neq q. \end{cases} \quad \textbf{(A.5)}$$

In terms of our notation, $\Phi^{j\to pq}(\omega_1, \omega_2)$ is the amplitude associated with photons 1 and 2 being coupled from input path j to output paths p and q, respectively. While the form of Eq. (A.4) is general, the $G^{j\to q}(\omega)$ will change if a different coupler architecture is used (such as an asymmetric coupler).

Two-photon outcome probabilities. The probability of finding photons 1 and 2 in output paths p and q, respectively, is calculated from $P_{pq} = \langle\Psi|\hat{b}^{p\dagger}\hat{b}^{q\dagger}\hat{b}^q\hat{b}^p|\Psi\rangle$ and found to be

$$P_{pq} = R_{pq}^C + \cos(\pi\delta_{pq})R_{pq}^I(\theta), \quad \textbf{(A.6)}$$

where δ_{pq} is the Kronecker delta,

$$R_{pq}^C = \int d\omega_1 d\omega_2(|\Phi^{A\to pq}(\omega_1, \omega_2)|^2 + |\Phi^{B\to pq}(\omega_1, \omega_2)|^2), \quad \textbf{(A.7)}$$

is the "classical" probability contributed by sources A and B in the absence of interference, and

$$R_{pq}^I(\theta) = \int d\omega_1 d\omega_2 2\,\text{Re}\{e^{-i\theta}\Phi^{B\to pq}(\omega_1, \omega_2)\Phi^{*A\to pq}(\omega_1, \omega_2)\}, \quad \textbf{(A.8)}$$

is a nonclassical modifier accounting for the effects of path interference. These expressions are given in their most general form so that they can be readily applied to any arbitrary set of coupler and two-photon state attributes. Note that $\sum_{pq} P_{pq} = 1$. The probability P_S of obtaining an antibunched (separated) outcome is then

$$P_S = P_{AB} + P_{BA} = P_S^C + P_S^I, \qquad \textbf{(A.9)}$$

with "classical" and "interference" components given by $P_S^C = R_{AB}^C + R_{BA}^C$ and $P_S^I = R_{AB}^I + R_{BA}^I$.

Obtaining V_S for on-chip measurement of Λ. We refer to the configuration shown in Fig. 7. Let $P_S(\Lambda, \tau)$ represent the total antibunched outcome probability at nondegeneracy Λ and relative time delay τ. Assuming $\eta(\lambda_{00}) = 0.5$ and $\theta = 0$, $P_S(\Lambda, 0) = 1$ at all values of Λ. The coincidence detection rate R_0 at zero delay therefore corresponds to maximum separation fidelity; thus the probability of pair separation at nonzero delay τ can be obtained from $P_S(\Lambda, \tau) = R_\tau/R_0$. Provided τ is large enough that $|\psi\rangle_A$ and $|\psi\rangle_B$ (the possible photon-pair histories) are no longer coherent, quantum interference will not occur at that delay time; thus, $P_S^I(\Lambda, \tau) = 0$ and $P_S(\Lambda, \tau) = P_S^C(\Lambda, \tau)$. It then follows from the definition of V_S that

$$V_S = \frac{|P_S(\Lambda, 0) - P_S(\Lambda, \tau)|}{P_S(\Lambda, \tau)} = \frac{|1 - R_\tau/R_0|}{R_\tau/R_0} = \left| \frac{R_0}{R_\tau} - 1 \right|.$$

$$\textbf{(A.10)}$$

For $\eta(\lambda_{00}) = 0.5$, the visibility V_S maps to a unique value of $M\Lambda$ provided $M\Lambda \le \pi/2$ [due to periodicity of V_S; see Fig. 4(d)].

See Supplement 1 for supporting content.

REFERENCES

1. H.-K. Lo, M. Curty, and B. Qi, "Measurement-device-independent quantum key distribution," Phys. Rev. Lett. **108**, 130503 (2012).
2. X. song Ma, B. Dakic, W. Naylor, A. Zeilinger, and P. Walther, "Quantum simulation of the wavefunction to probe frustrated heisenberg spin systems," Nature Phys. **7**, 399–405 (2011).
3. G. B. Lemos, V. Borish, G. D. Cole, S. Ramelow, R. Lapkiewicz, and A. Zeilinger, "Quantum imaging with undetected photons," Nature **512**, 409–412 (2014).
4. F. Schlawin, K. E. Dorfman, B. P. Fingerhut, and S. Mukamel, "Suppression of population transport and control of exciton distributions by entangled photons," Nat. Commun. **4**, 1782 (2013).
5. I. J. Luxmoore, R. Toro, O. D. Pozo-Zamudio, N. A. Wasley, E. A. Chekhovich, A. M. Sanchez, R. Beanland, A. M. Fox, M. S. Skolnick, H. Y. Liu, and A. I. Tartakovskii, "III-V quantum light source and cavity-qed on silicon," Sci. Rep. **3**, 1239 (2013).
6. M. Davanço, J. R. Ong, A. B. Shehata, A. Tosi, I. Agha, S. Assefa, F. Xia, W. M. J. Green, S. Mookherjea, and K. Srinivasan, "Telecommunications-band heralded single photons from a silicon nanophotonic chip," Appl. Phys. Lett. **100**, 261104 (2012).
7. N. Matsuda, H. L. Jeannic, H. Fukuda, T. Tsuchizawa, W. J. Munro, K. Shimizu, K. Yamada, Y. Tokura, and H. Takesue, "A monolithically integrated polarization entangled photon pair source on a silicon chip," Sci. Rep. **2**, 817 (2012).
8. R. T. Horn, P. Kolenderski, D. Kang, P. Abolghasem, C. Scarcella, A. D. Frera, A. Tosi, L. G. Helt, S. V. Zhukovsky, J. E. Sipe, G. Weihs, A. S. Helmy, and T. Jennewein, "Inherent polarization entanglement generated from a monolithic semiconductor chip," Sci. Rep. **3**, 2314 (2013).
9. J. C. F. Matthews, A. Politi, A. Stefanov, and J. L. O'Brien, "Manipulation of multiphoton entanglement in waveguide quantum circuits," Nat. Photonics **3**, 346–350 (2009).
10. P. J. Shadbolt, M. R. Verde, A. Peruzzo, A. Politi, A. Laing, M. Lobino, J. C. F. Matthews, M. G. Thompson, and J. L. O'Brien, "Generating, manipulating and measuring entanglement and mixture with a reconfigurable photonic circuit," Nat. Photonics **6**, 45–49 (2012).
11. J. Wang, A. Santamato, P. Jiang, D. Bonneau, E. Engin, J. W. Silverstone, M. Lermer, J. Beetz, M. Kamp, S. Höfling, M. G. Tanner, C. M. Natarajan, R. H. Hadfield, S. N. Dorenbos, V. Zwiller, J. L. O'Brien, and M. G. Thompson, "Gallium arsenide (GaAs) quantum photonic waveguide circuits," Opt. Commun. **327**, 49–55 (2014).
12. J. W. Silverstone, D. Bonneau, K. Ohira, N. Suzuki, H. Yoshida, N. Iizuka, M. Ezaki, C. M. Natarajan, M. G. Tanner, R. H. Hadfield, V. Zwiller, G. D. Marshall, J. G. Rarity, J. L. O'Brien, and M. G. Thompson, "On-chip quantum interference between silicon photon-pair sources," Nat. Photonics **8**, 104–108 (2014).
13. W. H. P. Pernice, C. Schuck, O. Minaeva, M. Li, G. Goltsman, A. Sergienko, and H. Tang, "High-speed and high-efficiency travelling wave single-photon detectors embedded in nanophotonic circuits," Nat. Commun. **3**, 1325 (2012).
14. G. Reithmaier, S. Lichtmannecker, T. Reichert, P. Hasch, K. Müller, M. Bichler, R. Gross, and J. J. Finley, "On-chip time resolved detection of quantum dot emission using integrated superconducting single photon detectors," Sci. Rep. **3**, 1901 (2013).
15. R. Horodecki, P. Horodecki, M. Horodecki, and K. Horodecki, "Quantum entanglement," Rev. Mod. Phys. **81**, 865–942 (2009).
16. P. Abolghasem, M. Hendrych, X. Shi, J. P. Torres, and A. S. Helmy, "Bandwidth control of paired photons generated in monolithic Bragg reflection waveguides," Opt. Lett. **34**, 2000 (2009).
17. A. Eckstein, A. Christ, P. J. Mosley, and C. Silberhorn, "Highly efficient single-pass source of pulsed single-mode twin beams of light," Phys. Rev. Lett. **106**, 013603 (2011).
18. D. Kang, A. Pang, Y. Zhao, and A. S. Helmy, "Two-photon quantum state engineering in nonlinear photonic nanowires," J. Opt. Soc. Am. B **31**, 1581–1589 (2014).
19. A. Yariv, "Coupled-mode theory for guided-wave optics," IEEE J. Quantum Electron. **9**, 919–933 (1973).
20. H. F. Taylor and A. Yariv, "Guided wave optics," Proc. IEEE **62**, 1044–1060 (1974).
21. S. Parker, S. Bose, and M. B. Plenio, "Entanglement quantification and purification in continuous-variable systems," Phys. Rev. A **61**, 032305 (2000).
22. T. S. Humble and W. P. Grice, "Effects of spectral entanglement in polarization-entanglement swapping and type-I fusion gates," Phys. Rev. A **77**, 022312 (2008).
23. Z. Yang, M. Liscidini, and J. E. Sipe, "Spontaneous parametric down-conversion in waveguides: A backward Heisenberg picture approach," Phys. Rev. A **77**, 033808 (2008).
24. T. H. Wood, "Multiple quantum well (MQW) waveguide modulators," J. Lightwave Technol. **6**, 743–757 (1988).
25. A. Stöhr, O. Humbach, S. Zumkley, G. Wingen, G. David, D. Jäger, B. Bollig, E. C. Larkins, and J. D. Ralston, "InGaAs/GaAs multiple-quantum-well modulators and switches," Opt. Quantum Electron. **25**, S865–S883 (1993).
26. M. J. F. Digonnet and H. J. Shaw, "Analysis of a tunable single mode optical fiber coupler," IEEE J. Quantum Electron. **18**, 746–754 (1982).
27. S. Hill and W. K. Wootters, "Entanglement of a pair of quantum bits," Phys. Rev. Lett. **78**, 5022–5025 (1997).
28. W. K. Wootters, "Entanglement of formation of an arbitrary state of two qubits," Phys. Rev. Lett. **80**, 2245–2248 (1998).
29. B. G. Christensen, K. T. McCusker, J. B. Altepeter, B. Calkins, T. Gerrits, A. E. Lita, A. Miller, L. K. Shalm, Y. Zhang, S. Nam, N. Brunner, C. C. Lim, N. Gisin, and P. G. Kwiat, "Detection-loophole-free test of quantum nonlocality, and applications," Phys. Rev. Lett. **111**, 130406 (2013).
30. F. Schlawin and S. Mukamel, "Two-photon spectroscopy of excitons with entangled photons," J. Chem. Phys. **139**, 244110 (2013).
31. A. Muthukrishnan, G. S. Agarwal, and M. O. Scully, "Inducing disallowed two-atom transitions with temporally entangled photons," Phys. Rev. Lett. **93**, 093002 (2004).
32. F. Schlawin and S. Mukamel, "Matter correlations induced by coupling to quantum light," Phys. Rev. A **89**, 013830 (2014).
33. C. K. Hong, Z. Y. Ou, and L. Mandel, "Measurement of subpicosecond time intervals between two photons by interference," Phys. Rev. Lett. **59**, 2044–2046 (1987).
34. T. B. Pittman, D. V. Strekalov, A. Migdall, M. H. Rubin, A. V. Sergienko, and Y. H. Shih, "Can two-photon interference be considered the interference of two photons?" Phys. Rev. Lett. **77**, 1917–1920 (1996).
35. D. V. Strekalov, T. B. Pittman, and Y. H. Shih, "What we can learn about single photons in a two-photon interference experiment," Phys. Rev. A **57**, 567–570 (1998).
36. J. Chen, K. F. Lee, and P. Kumar, "Deterministic quantum splitter based on time-reversed Hong-Ou-Mandel interference," Phys. Rev. A **76**, 031804 (2007).

37. H. Jin, F. Liu, P. Xu, J. Xia, M. Zhong, Y. Yuan, J. Zhou, Y. Gong, W. Wang, and S. Zhu, "On-chip generation and manipulation of entangled photons based on reconfigurable lithium-niobate waveguide circuits," Phys. Rev. Lett. **113**, 103601 (2014).

38. M. Avenhaus, A. Eckstein, P. J. Mosley, and C. Silberhorn, "Fiber-assisted single-photon spectrograph," Opt. Lett. **34**, 2873–2875 (2009).

39. R. Kumar, J. R. Ong, M. Savanier, and S. Mookherjea, "Controlling the spectrum of photons generated on a silicon nanophotonic chip," Nat. Commun. **5**, 5489 (2014).

40. R.-B. Jin, R. Shimizu, K. Wakui, H. Benichi, and M. Sasaki, "Widely tunable single photon source with high purity at telecom wavelength," Opt. Express **21**, 10659–10666 (2013).

41. X. Shi, A. Valencia, M. Hendrych, and J. P. Torres, "Generation of indistinguishable and pure heralded single photons with tunable bandwidth," Opt. Lett. **33**, 875–877 (2008).

42. A. Laing, A. Peruzzo, A. Politi, M. R. Verde, M. Halder, T. C. Ralph, M. G. Thompson, and J. L. O'Brien, "High-fidelity operation of quantum photonic circuits," Appl. Phys. Lett. **97**, 211109 (2010).

43. A. Takagi, K. Jinguji, and M. Kawachi, "Wavelength characteristics of (2x2) optical channel-type directional couplers with symmetric or nonsymmetric coupling structures," J. Lightwave Technol. **10**, 735–746 (1992).

44. G. S. Agarwal and S. D. Gupta, "Filtering of two-photon quantum correlations by optical cavities: Cancellation of dispersive effects," Phys. Rev. A **49**, 3954–3957 (1994).

45. Y. Bromberg, Y. Lahini, and Y. Silberberg, "Quantum and classical correlations in waveguide lattices," Phys. Rev. Lett. **105**, 263604 (2010).

46. N. Spagnolo, C. Vitelli, L. Aparo, P. Matalon, F. Sciarrino, A. Crespi, R. Ramponi, and R. Osellame, "Three-photon bosonic coalescence in an integrated tritter," Nat. Commun. **4**, 1606 (2013).

47. J. Chen, X. Li, and P. Kumar, "Two-photon-state generation via four-wave mixing in optical fibers," Phys. Rev. A **72**, 033801 (2005).